Supporting Information

The confined interlayer growth of ultrathin two-dimensional Fe_3O_4 nanosheets with enriched oxygen vacancies for peroxymonosulfate activation

Weixue Wang,[†,‡] Yang Liu,[†] Yifan Yue,[†] Huihui Wang,[†] Gong Cheng,[†] Chunyang Gao,[&] Chunlin Chen,[&] Yuejie Ai,[†] Zhe Chen,[†,] and Xiangke Wang[†]*

[†]MOE Key Laboratory of Resources and Environmental System Optimization, College of Environmental Science and Engineering, North China Electric Power University, Beijing 102206, P. R. China

[‡]School of Chemical Engineering, Northeast Electric Power University, Jilin 132000, P. R. China

[&]Shenyang National Laboratory for Materials Science, Institute of Metal Research, Chinese Academy of Sciences, Shenyang 110016, P. R. China

Table of Contents

1 Experimental Procedures

1.1 Sources of chemicals. All chemicals were of high-purity reagent grade and used without further purification. $FeCl_3•6H_2O$, NaOH, commercial Fe_3O_4, *tert*-butanol (TBA), ethanol, methanol, deuterium oxide (D_2O), p-benzoquinone (p-BQ), bisphenol A (BPA), 2-chlorophenol, 4-chlorophenol, 2,4-dichlorophenol, 2,4,6-trichlorophenol, phenol, tetracycline, ofloxacin, ciprofloxacin, diphenhydramine and benzoic acid were all purchased from Aladdin Company. Peroxymonosulfate (PMS, $KHSO_5•0.5KHSO_4•0.5K_2SO_4$) was purchased from Alfa Aesar. Acetone was purchased from Sinopharm Co., Ltd. All the aqueous solutions were prepared by using Milli-Q water.

1.2 Template preparation. The RUB-15 (a zeolite precursor as laminar template) was synthesized according to the procedure described by Moteki et al.[1]

1.3 Catalyst preparation. To prepare a typical catalyst, a certain mass of $FeCl_3•6H_2O$ and template RUB-15 were mechanical mixed uniformly. The mass ratio of $FeCl_3•6H_2O$ and RUB-15 was varied from 0.1:1 ~ 20:1. Afterwards, the mixture was heated to 450° C at a rate of 5° C/min under Ar atmosphere, and kept under 450° C for 60 min. After cooling down to room temperature, the mixture was washed with acetone until the supernatant was colorless. Finally, template RUB-15 was etched by NaOH solution (1 M). After thorough washing and freeze drying, the 2D Fe_3O_4 was obtained. In contrast, the template-free sample consisted entirely of $FeCl_3•6H_2O$ was labeled as Fe_2O_3-without-template.

1.4 Characterization. Powder X-ray diffraction patterns were collected on SmartLab SE (XRD, Rigaku) equipped with Cu-Kα (λ = 1.54 Å) radiation at a scanning rate of 2°/min over the range of 2°−80° (2θ). Raman spectra were scanned on Invia (Renishaw) with 40 mW at 633 nm laser light irradiation. The specific surface area was analyzed by N_2 adsorption-desorption isotherms measured at 77 K (ASAP2460,

Micromeritics). The samples were outgassed at 50 mTorr and 120° C for 12 h prior to analysis. The morphology was characterized by field-emission scanning electron microscopy (SEM, Hitachi SU8010) and high-resolution transmission electron microscopy (TEM, Tecnai G^2 F20). The Figure 2a, b, d were generated on a CS-corrected high-resolution transmission electron microscope (CS-corrected HRTEM, Titan Cubed Themis G3 300). Atomic force microscope image was performed on 5500AFM (AFM, Aglient Keysight), and the samples were dispersed on mica plate for the test. ^{57}Fe Mössbauer spectrum was obtained at room temperature with a constant acceleration on Mössbauer spectrometer (Wissel, Germany), using ^{75}Co(Pd) as radioactive source. X-ray photoelectron spectroscopy measurements were taken in 250 xi (XPS, Thermo ESCALAB) using a monochromatic Al Kα X-ray source. The oxygen temperature-programmed desorption (O_2-TPD) was performed on Auto Chem II 2920. An approximately 120 mg sample was dry pretreated under flowing He (50 mL/min) at a rate of 10° C/min to 300° C and kept for 2 h, then cooled down naturally. After that, gas mixture O_2/He (50 mL/min) was injected for 1 h to reach adsorption saturation and switched to flowing He (50 mL/min) for 1 h to remove surface weak physical adsorption of O_2. Then continue heating up to 700° C at a rate of 10° C/min, the effluent gas was analyzed online using thermal conductivity detector. The Fe K-edge X-ray absorption fine structure (XAFS) spectra were taken at Shanghai Synchrotron Radiation Facility (SSRF, BL14W1 line-station) with 32-element Ge detector in fluorescence mode. The ATHENA and ARTEMIS packages of IFEFFIT software were employed to normalize and simulate the EXAFS data, respectively.[2,3] The crystallographic data of magnetite was used as the reference for the coordination environment between iron and oxygen atoms in the first shell,[4] commercial Fe_3O_4 was purchased from Aladdin Company. Low temperature electron paramagnetic resonance (EPR) of solid sample was taken on Bruker-A300-10/12

spectrometer and measured at 77 K. In addition, the EPR signals of radicals were also examined on Bruker-A300-10/12 spectrometer at room temperature. The concentration of iron ions in solution was quantified by inductively coupled plasma optical emission spectrometry (ICP-OES, Optima 5300 DV, Perkin Elmer). The total organic carbon (TOC) was measured on Multi N/C 3100 (Analytik Jena).

1.5 Experimental procedure and analytical methods. The Fenton-like catalytic performance was assessed at 25° C using a water bath. Typically, 10 mg catalyst was added into 50 mL reaction mixture ([organic compounds] = 20 mg/L) and stirred for 30 min to establish the adsorption-desorption equilibrium. The pH was adjusted to targeted value by using 0.1 M HCl or 0.1 M NaOH solution. The catalyticreaction was initiated by adding a certain amount of PMS. At predetermined time intervals, the reaction solution was filtered through a polyether sulfone membrane (pore size 0.45 μm). The concentration of organic pollutant was analyzed immediately by high performance liquid chromatography (HPLC, Agilent, 1260-Infinity).

1.6 Electrochemical analysis tests. The electrochemical analysis was carried out on electrochemical workstation (Metrohm PGSTAT302N). All the experiments were conducted with three-electrode-cell configuration including a working electrode, a platinum electrode as counter electrode, and a Ag/AgCl electrode as reference electrode. Electrochemical impedance spectroscopy (EIS) of Nyquist plots using catalyst-coated ITO conductive glass electrode as working electrode, which were measured in aqueous Na_2SO_4 solution (0.5 M). The open circuit potentials were monitored by chronopotentiometry (CP) analysis and using a catalyst-coated glassy carbon electrode (GCE) as working electrode, which was performed from −0.1 V to +1.0 V at a scan rate of 10 mVs^{-1}.

1.7 Density functional theory calculations. All the geometry relaxation and electronic characteristic calculations were performed using density functional theory (DFT)

calculations via Vienna *ab initio* Simulation Package (VASP) with plane-wave projector-augmented wave (PAW) pseudopotentials.[5,6] The function of Generalized Gradient Approximation (GGA) with Pedrew-Burke-Ernzerhof (PBE) was applied to deal with the exchange correlation energy.[7] The cutoff energy was chosen as 400 eV and the Monkhorst-Pack mesh k-points was set to 1×1×1 in the calculations. Meanwhile, all atoms could be relaxed until the energy iteration of two consecutively geometric optimization steps was less than 10^{-5} eV, and the convergence tolerance of Hellmann-Feynman force on each atom was 0.02 eV/Å. The unit cell of Fe_3O_4 with a lattice constant of a = b = c = 8.533 Å, $\alpha = \beta = \gamma = 90°$ was chosen as the computational model in this calculation, and the spin polarization was also taken into consideration due to the strong antiferromagnetic coupling between the tetrahedral Fe ions and octahedral Fe ions.[8,9] The Fe_3O_4 (111) surface was studied in present work since it was the dominant cleavage plane of magnetite as proposed in previous researches. The Fe_3O_4 (111) surface had six different terminations which could be named as Fe_{tet1}, O_1, Fe_{oct1}, O_2, Fe_{tet2}, Fe_{oct2} (Figure S9a).[10] Previous theoretical studies have demonstrated that the Fe_{tet1} and Fe_{oct2} terminations were the most stable species.[11] Herein, we further performed geometric optimizations which showed that Fe_{oct2}-termination (−206.77660066 eV) was more stable than Fe_{tet1}-termination (−206.74434675 eV). Thus, we used Fe_{oct2}-termination along with [111] direction in the following simulation. Four kinds of computational models including less layers Fe_3O_4 (l-Fe_3O_4), multiple layers Fe_3O_4 (m-Fe_3O_4), less layers Fe_3O_4 enriched of oxygen vacancies (l-Fe_3O_4-OV) and multiple layers Fe_3O_4 enriched of oxygen vacancies (m-Fe_3O_4-OV) were constructed to distinguish the effect of thickness and oxygen defects. The constructed computational models were 2×2 supercell, and the thickness of less layers Fe_3O_4 and multiple layers Fe_3O_4 were about 8 Å and 18 Å, respectively. A 20 Å of vacuum on Z direction was added to avoid the interaction of adjacent period. In terms of the oxygen vacancies, two possible sites (vacancy 1 and vacancy 2) on Fe_{oct2}-termination were shown in Figure S9b，and the calculated results

showed that vacancy 2 (−819.23275667 eV) were more stable than vacancy 1 (−818.71934629 eV), so we focused on vacancy 2 in the following study. Then the adsorption configuration and bader charge of BPA-Fe_3O_4 systems were investigated to simulate the interfacial charge transfer trend of different models.

2 Results and Discussion

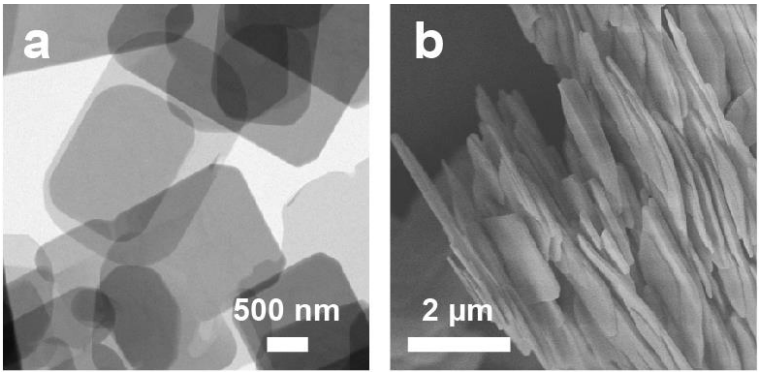

Figure S1. (a) TEM image and (b) SEM image of template RUB-15.

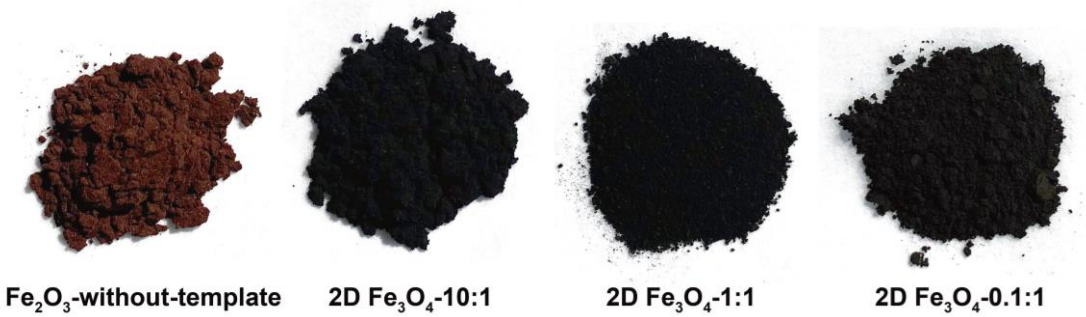

Figure S2. Photograph of the as-prepared samples.

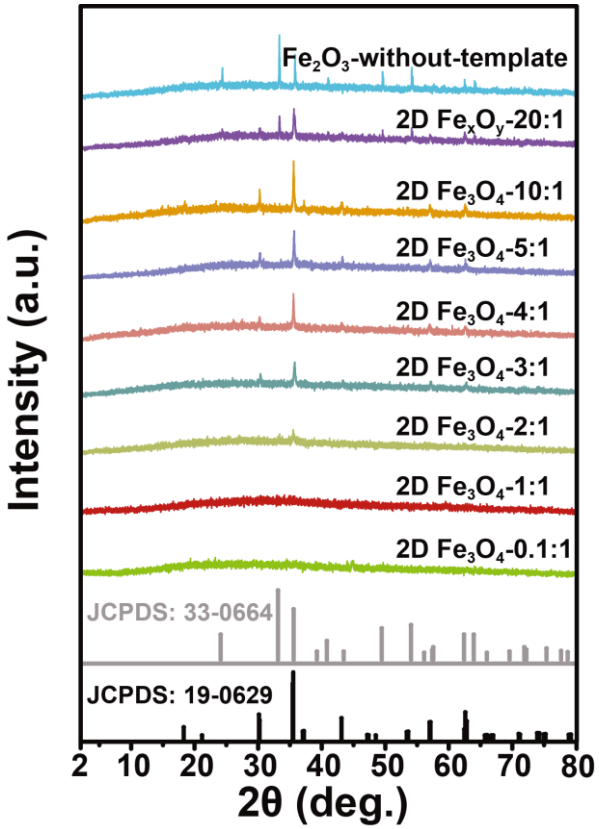

Figure S3. XRD patterns of samples with different proportion.

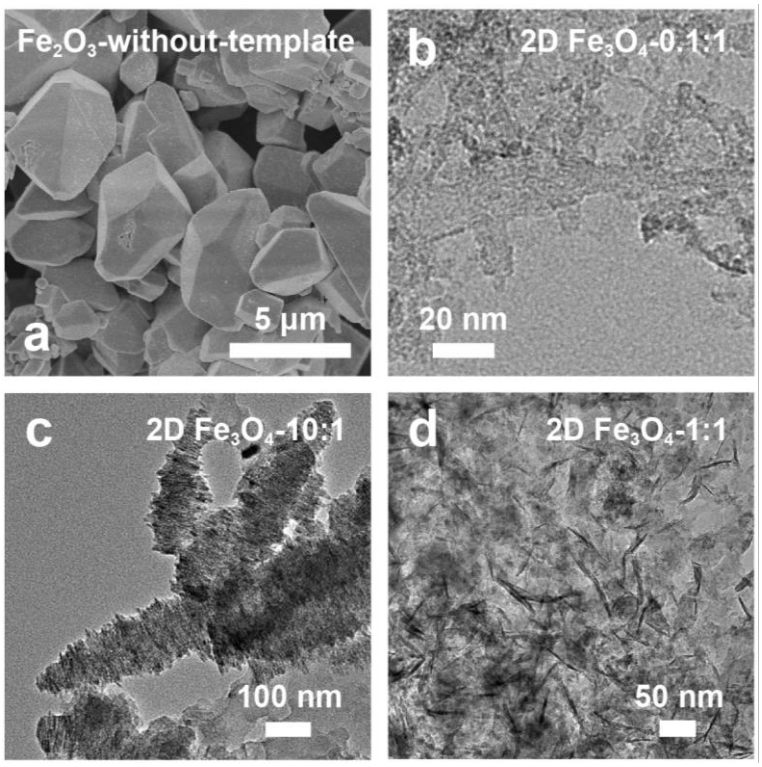

Figure S4. Morphology of the as-prepared samples (a) SEM image of Fe_2O_3-without-template, TEM images of (b) 2D Fe_3O_4-0.1:1, (c) 2D Fe_3O_4-10:1, (d) 2D Fe_3O_4-1:1.

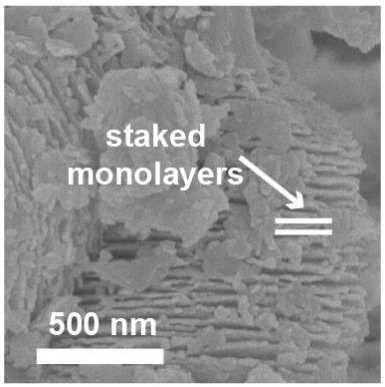

Figure S5. SEM image of 2D Fe_3O_4-1:1.

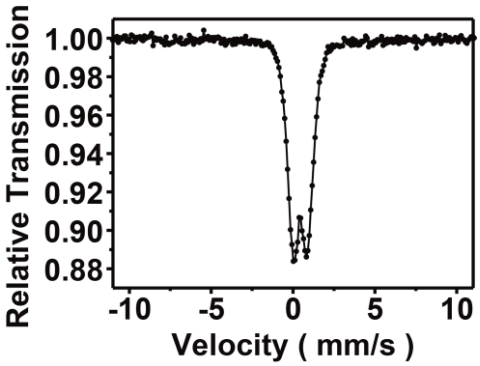

Figure S6. Mössbauer spectrum of 2D Fe_3O_4-1:1 at room temperature.

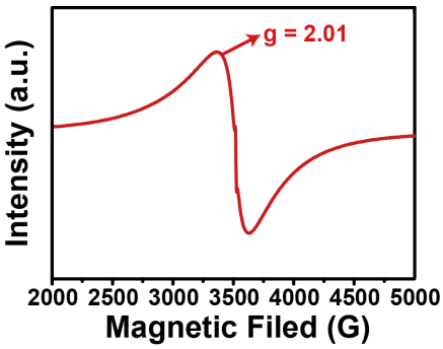

Figure S7. Low temperature EPR spectra of 2D Fe_3O_4-1:1.

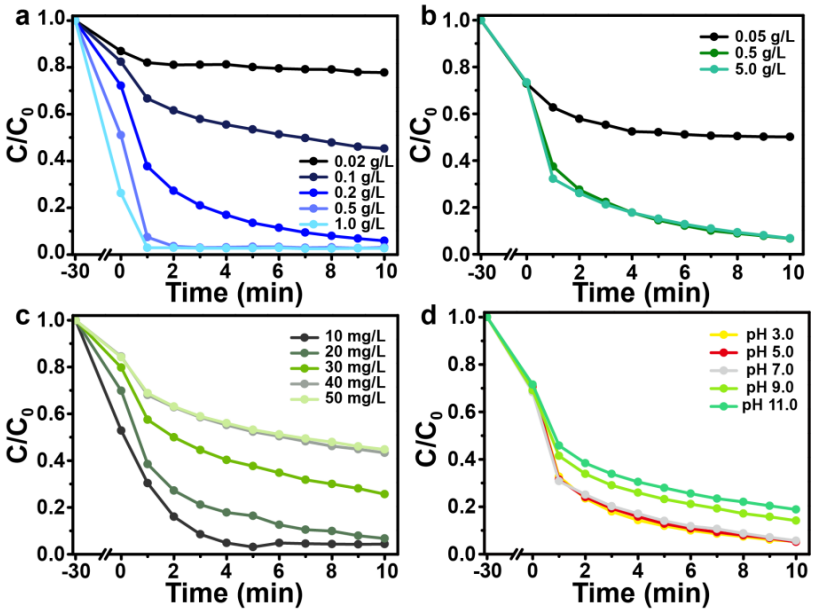

Figure S8. Effects of (a) catalyst dose, (b) oxidant dose, (c) the initial concentration of BPA and (d) various pH conditions during the degradation of BPA in 2D Fe_3O_4-1:1/PMS system. (reaction condition: [BPA] = 10−50 mg/L, [catalyst] = 0.02−1.0 g/L, [PMS] = 0.05−5.0 g/L, T = 25° C, initial solution pH = 3.0−11.0, reaction time = 10 min)

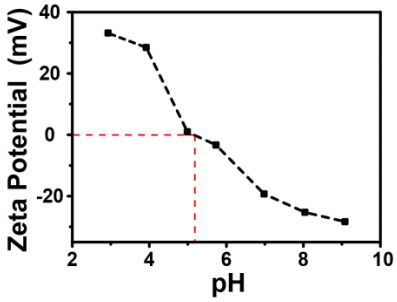

Figure S9. Zeta potential of 2D Fe_3O_4-1:1 as a function of pH.

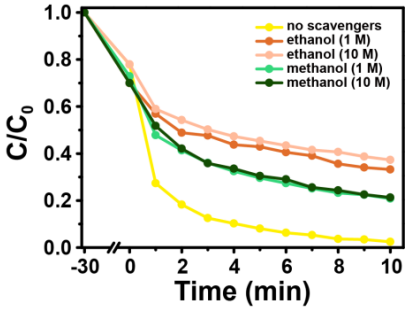

Figure S10. Effects of ethanol and methanol dose on the degradation of BPA in 2D Fe_3O_4-1:1/PMS system. (reaction condition: [BPA] = 20 mg/L, [catalyst] = 0.2 g/L, [PMS] = 0.5 g/L, T = 25° C, initial solution pH = 6.0, reaction time = 10 min)

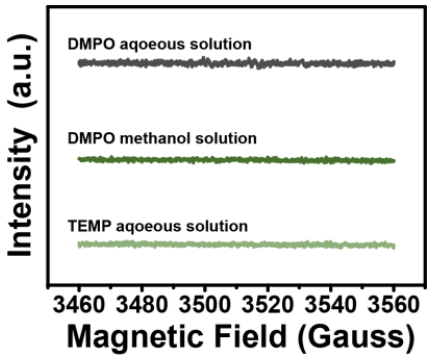

Figure S11. EPR of the autolysis by PMS in the absence of catalyst at 30 s.

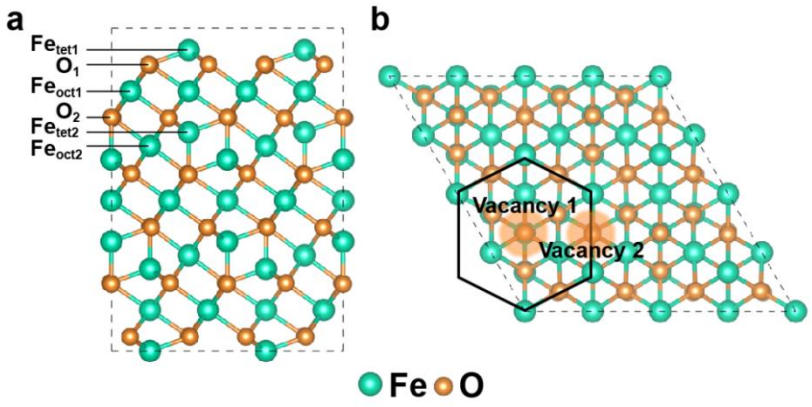

Figure S12. (a) Six terminations along the [111] direction on Fe_3O_4, (b) the possible oxygen vacancies on Fe_{oct2}-termination.

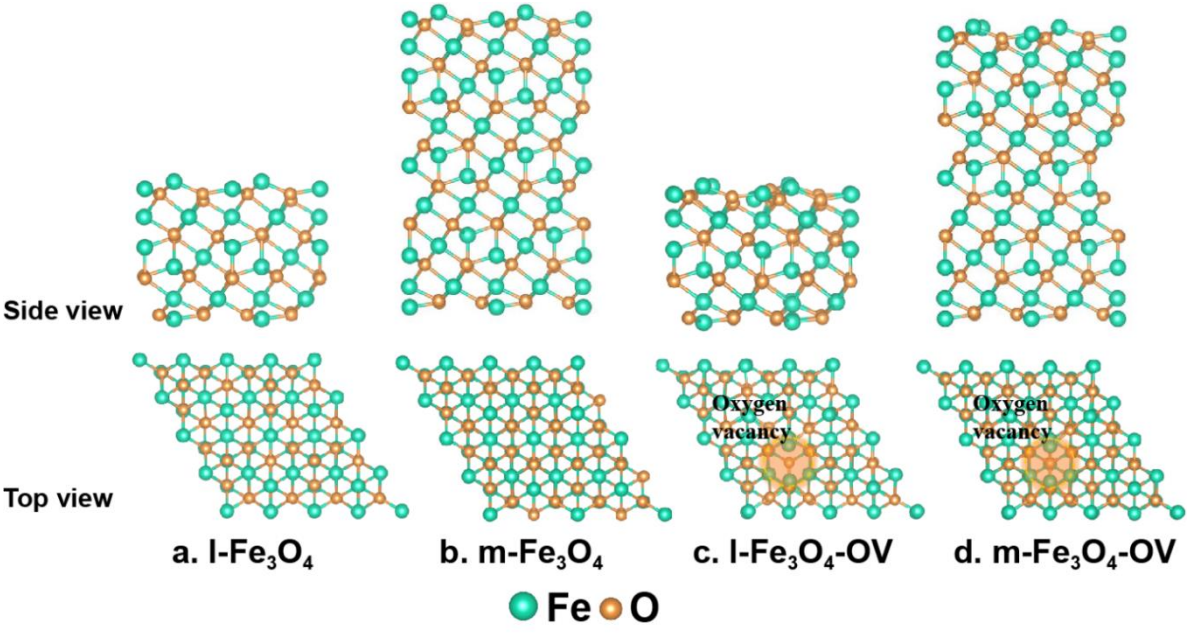

Figure S13. The optimized geometric structures of (a) l-Fe_3O_4, (b) m-Fe_3O_4, (c) l-Fe_3O_4-OV and (d) m-Fe_3O_4-OV.

Table S1. Chemical formulas and detailed information for HPLC analysis.

Compounds	Formula	Mobile phase (%)					
		Milli-Q water	Milli-Q water (0.08% H_3PO_4)	Milli-Q water (0.02M Na_3PO_4)	Methanol	Acetonitrile	Wavelength (nm)
bisphenol A	$C_{15}H_{16}O_2$	30			70		225
2-chlorophenol	ClC_6H_4OH	40			60		275
4-chlorophenol	C_6H_5OCl	30			70		280
2,4-dichlorophenol	$C_6H_4Cl_2O$	30			70		220
2,4,6-trichlorophenol	$C_6H_3Cl_3O$	30			70		290
phenol	C_6H_5OH	40			60		275
tetracycline	$C_{22}H_{24}N_2O_8$	75			25		375
ofloxacin	$C_{18}H_{20}FN_3O_4$		85			15	288
ciprofloxacin	$C_{17}H_{18}FN_3O_3$		80			20	278
diphenhydramine	$C_{17}H_2NO$		50			50	221
benzoic acid	$C_7H_6O_2$			75	25		254

Table S2. The Brunauer-Emmett-Teller specific surface areas and total pore volumes.

Entry	BET specific surface areas (m^2/g)	total pore volumes (cm^3/g)
Fe_2O_3-withou-template	7.91	0.03
2D Fe_3O_4-10:1	57.50	0.12
2D Fe_3O_4-1:1	132.40	0.21
2D Fe_3O_4-0.1:1	383.61	0.46

Table S3. XPS peaks binding energies and the relevant ratios.

Entry	Binding Energy of O 1s (eV)			Binding Energy of Fe 3p (eV)		Fe^{2+}/Fe^{3+}	O_{ads}/O_{total} (at.%)	OVs (%)
	Relative ratios (%)			Relative ratios (%)				
	O_{latt}	O_{ads}	O_{surf}	Fe^{2+}	Fe^{3+}			
commercial Fe_3O_4	529.85	531.13	532.68	54.90	55.70	0.50	24.26	0.00
	72.04	24.26	3.70	33.41	66.59			
2D Fe_3O_4-10:1	530.02	531.56	533.05	54.99	55.74	0.55	26.25	0.83
	67.65	26.25	6.10	35.52	64.48			
2D Fe_3O_4-1:1	530.47	531.90	533.80	55.50	56.25	0.70	39.43	2.99
	47.79	39.43	12.78	41.06	58.94			
2D Fe_3O_4-0.1:1	530.40	531.64	533.21	55.52	56.27	0.65	38.63	2.31
	48.73	38.63	12.64	39.36	60.64			

Table S4. The Fenton-like catalytic performance comparison of recently reported catalysts for PMS activation.

Catalyst	Persistent organic pollutants	Pollutant concentration	PMS dose	Catalyst dose	Reaction time	Conv. (%)	k (min^{-1})	Ref.
prussian blue analogues in the interlayers of layered double hydroxides (PBA-LDH)	carbamazepine	20 mg/L	0.5 mM	0.2 g/L	15 min	100	——	12
magnetic epigallocatechin-3-gallate-modified Fe_3O_4 nano-catalyst (EGCG@Fe_3O_4)	sulfadiazine	0.04 mM	0.3 mM	0.8 g/L	60 min	67.8	0.0541	13
kaolinite	atrazine	4.6 μM	1.0 mM	1.0 g/L	60 min	＞90	——	14
$CuFe_2O_4$/CuO	iopromide	1 μM	20 μM	100 mg/L	10 min	＞70	——	15
$CoFe_2O_4$	di-n-butyl phthalate	2 μM	0.02 mM	0.1 g/L	30 min	＞81.0	——	16
$CuFe_2O_4$	bisphenol A	50 mg/L	0.5 g/L	0.4 g/L	60 min	95.2	——	17
MnFeO	bisphenol A	10 mg/L	0.2 g/L	0.1 g/L	30 min	＞95	0.10	18
$LaFeO_3$	diclofenac	0.025 mM	0.5 mM	0.1 g/L	30 min	100	0.0833	19
$La_{0.4}Sr_{0.6}MnO_{3-\delta}$ (LSMO46)	phenol	0.2 mM	6.5 mM	0.2 g/L	90 min	100	0.0308	20
Fe/Fe_3C	phenol	0.2 mM	6.5 mM	0.2 g/L	60 min	100	0.0396	20
2D Fe_3O_4-1:1	bisphenol A	20 mg/L	0.5 g/L	0.2 g/L	10 min	93.2	0.2221	This work

References

(1) Moteki, T.; Chaikittisilp, W.; Sakamoto, Y.; Shimojima, A.; Okubo, T. Role of acidic pretreatment of layered silicate RUB-15 in its topotactic conversion into pure silica sodalite, *Chem. Mater.* **2011**, *23*, 3564−3570.

(2) Newville, M. EXAFS analysis using FEFF and FEFFIT, *J. Synchrotron Radiat.* **2001**, *8*, 96−100.

(3) Ravel,B.; Newville, M. ATHENA, ARTEMIS, HEPHAESTUS: Data analysis for X-ray absorption spectroscopy using IFEFFIT, *J. Synchrotron Radiat.* **2005**, *12*, 537−541.

(4) Haavik, C.; Stølen, S.; Fjellvåg, H.; Hanfland, M.; Häusermann, D. Equation of state of magnetite and its high-pressure modification: Thermodynamics of the Fe-O system at high pressure, *Am. Mineral.* **2000**, *85*, 514–523.

(5) Kresse, G.; Furthmüller, J. Efficiency of ab-initio total energy calculations for metals and semiconductors using a plane-wave basis set, *Comput. Mater. Sci.* **1996**, *6*, 15−50.

(6) Kresse, G.; Joubert, D. From ultrasoft pseudopotentials to the projector augmented-wave method, *Phys. Rev. B* **1999**, *59*, 1758−1775.

(7) Perdew, J. P.; Burke, K.; Ernzerhof, M. Generalized gradient approximation made simple, *Phys. Rev. Lett.* **1996**, *77*, 3865−3868.

(8) Yu, X.; Huo, C. F.; Li, Y. W.; Wang, J.; Jiao, H. Fe_3O_4 surface electronic structures and stability from GGA + U, *Surf. Sci.* **2012**, *606*, 872−879.

(9) Xue, P.; Fu, Z.; Yang, Z. The density functional theory studies on the promoting effect of the Cu-modified Fe_3O_4 catalysts, *Phys. Lett. A* **2015**, *379*, 607−612.

(10) Weiss, W.; Ranke, W. Surface chemistry and catalysis on well-defined epitaxial iron-oxide layers, *Prog. Surf. Sci.* **2002**, *70*, 1−151.

(11) Zhu, L.; Yao, K. L.; Liu, Z. L. First-principles study of the polar (111) surface of Fe_3O_4, *Phys. Rev. B* **2006**, *74*, 035409.

(12) Zeng, H.; Deng, L.; Shi, Z.; Luo, J.; Crittenden, J. Heterogeneous degradation of carbamazepine by Prussian blue analogues in the interlayers of layered double hydroxides: Performance, mechanism and toxicity evaluation, *J. Mater. Chem. A* **2019**, *7*, 342−352.

(13) Tan, C.; Jian, X.; Dong, Y.; Lu, X.; Liu, X.; Xiang, H.; Cui, X.; Deng, J.; Gao, H. Activation of peroxymonosulfate by a novel EGCE@Fe_3O_4 nanocomposite: Free radical reactions and implication for the degradation of sulfadiazine, *Chem. Eng. J.* **2019**, *359*, 594−603.

(14) Li, C.; Huang, Y.; Dong, X.; Sun, Z.; Duan, X.; Ren, B.; Zheng, S.; Dionysiou, D. D. Highly efficient activation of peroxymonosulfate by natural negatively charged kaolinite with abundant hydroxyl groups for the degradation of atrazine, *Appl. Catal. B Environ.* **2019**, *247*, 10−23.

(15) Zhang, T.; Zhu, H.; Croué, J. P. Production of sulfate radical from

peroxymonosulfate induced by a magnetically separable $CuFe_2O_4$ spinel in water: Efficiency, stability, and mechanism, *Environ. Sci. Technol.* **2013**, *47*, 2784−2791.

(16) Ren, Y.; Lin, L.; Ma, J.; Yang, J.; Feng, J.; Fan, Z. Sulfate radicals induced from peroxymonosulfate by magnetic ferrospinel MFe_2O_4 (M = Co, Cu, Mn, and Zn) as heterogeneous catalysts in the water, *Appl. Catal. B Environ.* **2015**, *165*, 572−578.

(17) Xu, Y.; Ai, J.; Zhang, H. The mechanism of degradation of bisphenol A using the magnetically separable $CuFe_2O_4$/peroxymonosulfate heterogeneous oxidation process, *J. Hazard. Mater.* **2016**, *309*, 87−96.

(18) Huang, G. X.; Wang, C. Y.; Yang, C. W.; Guo, P. C.; Yu, H. Q. Degradation of bisphenol A by peroxymonosulfate catalytically activated with $Mn_{1.8}Fe_{1.2}O_4$ nanospheres: Synergism between Mn and Fe, *Environ. Sci. Technol.* **2017**, *51*, 12611−12618.

(19) Rao, Y.; Zhang, Y.; Han, F.; Guo, H.; Huang, Y.; Li, R.; Qi, F.; Ma, J. Heterogeneous activation of peroxymonosulfate by $LaFeO_3$ for diclofenac degradation: DFT-assisted mechanistic study and degradation pathways, *Chem. Eng. J.* **2018**, *352*, 601−611.

(20) Miao, J.; Duan, X.; Li, J.; Dai, J.; Liu, B.; Wang, S.; Zhou, W.; Shao, Z. Boosting performance of lanthanide magnetism perovskite for advanced oxidation through lattice doping with catalytically inert element, *Chem. Eng. J.* **2019**, *355*, 721−730.